

Universal electrical transport of composite Fermi liquid to Metal transition in Moiré systems

Youxuan Wang, Rongning Liu, Feng Liu, and Xue-Yang Song

Department of Physics, The Hong Kong University of Science and Technology, Clear Water Bay, Hong Kong, China

We compute universal electrical transport near continuous transitions between a composite Fermi liquid (CFL) and a metallic phase in moiré Chern bands, focusing on fillings $\nu = -1/2$ and $\nu = -3/4$. The critical theory represents a novel QED–Chern–Simons framework: a charged sector at a bosonic Laughlin–superfluid critical point is coupled, via emergent gauge fields and Chern–Simons mixing, to a neutral spinon Fermi surface. Integrating out matter fields to quadratic order yields an explicit Ioffe–Larkin composition rule for the full resistivity tensor, showing how longitudinal channels add in series while Chern–Simons terms generate Hall response. To obtain the DC limit in the quantum critical fan, we develop a controlled large- N expansion where both fermion flavors and Chern–Simons levels scale with N , and solve a quantum Boltzmann equation at leading nontrivial order $1/N$. Gauge-mediated inelastic scattering removes the collisionless Drude singularity and produces a universal scaling function $\Sigma(\omega/T)$ and finite DC conductivities $\sigma(0) \approx 0.033(e^2/\hbar)$ ($\nu = -1/2$) and $0.047(e^2/\hbar)$ ($\nu = -3/4$). We also identify a Chern–Simons “filtering” mechanism that suppresses transmission of Landau damping from the spinon Fermi surface to the critical gauge mode. Our approach provides concrete transport diagnostics for detecting quantum criticality in moiré superlattices.

I. INTRODUCTION

Moiré superlattices provide a highly tunable platform where strong electronic correlations coexist with nontrivial band topology. In several transition-metal dichalcogenide (TMD) and graphene-based moiré systems[1, 2], narrow isolated Chern bands can be realized at (nearly) zero external magnetic field, enabling the observation of integer and fractional quantum anomalous Hall (FQAH) states[3–7], extensively studied by a number of theoretical works[8–22]. Furthermore numerical evidence of composite Fermi liquid in valley polarized Moiré TMD systems is reported at filling $1/2$ and $3/4$ [23, 24] in line with the picture of a Chern band mimicking the lowest Landau level. A key capability that distinguishes moiré systems from conventional Landau-level settings is the ability to tune the effective bandwidth (for example via a perpendicular displacement field) while keeping the interaction scale comparatively fixed[1, 25]. This makes it possible to access continuous evolutions—and potentially quantum critical points—between quantum Hall-like phases and more conventional metallic or charge-ordered phases at fixed lattice filling.

Motivated by these developments, Song, Zhang, and Senthil[26] constructed effective field theories for unconventional phase transitions out of quantum Hall states in moiré Chern bands. A central organizing idea is a parton description in which the physical electron is fractionalized into a charged sector and a neutral Fermi-surface sector, coupled by an emergent gauge field[27, 28]. In this framework, the quantum Hall or composite Fermi liquid (CFL) phenomenology is encoded in a strongly correlated charged sector, while metallic degrees of freedom can persist in a neutral sector; their coupling through gauge fluctuations allows one to describe transitions between a CFL and a conventional Fermi liquid (FL) in a unified way[29, 30].

In this work we focus on the CFL–FL transition at filling $\nu = -3/4$, for which Ref. [26] proposed a quantum critical theory built from (i) a critical charged sector associated with a bosonic Laughlin–superfluid transition at effective filling $1/4$ [31, 32], and (ii) a neutral Fermi surface, “glued” together by emergent gauge fields and Chern–Simons couplings[33]. While the detailed microscopic realization is specific to moiré Chern bands, the resulting low-energy theory is an example of “beyond-Landau” criticality, closely related in structure to deconfined quantum critical points[34–36] but enriched by topological response terms.

Understanding charge transport in the vicinity of this transition is important for two reasons. First, electrical resistivities provide direct experimental diagnostics for identifying the critical regime and distinguishing it from nearby metallic or insulating phases. In particular, the coupling between the critical charged sector and the neutral Fermi surface implies that the observable conductivity is a nontrivial composition of multiple sectors rather than the response of a single quasiparticle band. Second, quantum critical transport in $(2+1)$ dimensions is controlled by universal scaling functions of ω/T and is sensitive to the interplay between emergent gauge fluctuations and critical matter[37]. A controlled computation of the conductivity therefore sharpens the connection between the effective field theory and experimentally accessible signatures in moiré materials, and clarifies which features are universal consequences of the proposed CFL–FL critical point.

Our goal is to compute the *low-frequency* electrical transport in the quantum critical regime of the CFL–FL transition. A crucial general lesson from quantum critical transport is that the limits $\omega \rightarrow 0$ and $T \rightarrow 0$ do *not* commute: a strictly $T = 0$ Kubo calculation captures the collisionless response at $\omega/T \rightarrow \infty$, whereas the DC conductivity is controlled by the hydrodynamic

regime $\omega/T \rightarrow 0$ and requires a finite- T treatment of inelastic scattering. This was emphasized in the seminal work of Damle and Sachdev on $(2+1)$ -dimensional interacting QCPs [37, 38], and appears in a particularly sharp way in fractionalized critical theories where gauge fluctuations generate strong, universal scattering channels at nonzero temperature[39, 40].

Our starting point is the critical Lagrangian proposed in Ref. [26], which decomposes the electron into a charged critical sector and a neutral Fermi-surface sector coupled by emergent gauge fields and Chern–Simons terms. Because the physical probe field couples only through gauge-invariant combinations, the linear electromagnetic response can be obtained efficiently by integrating out the matter fields to quadratic order and solving the resulting Gaussian gauge theory. This yields an *Ioffe–Larkin composition rule* for the full polarization tensor (equivalently for the conductivity/resistivity tensor), which expresses the physical resistivity as a “series connection” of the resistive channels associated with the partons and the Chern–Simons sector [41]. In practice, this step reduces the transport problem to determining the response functions of the critical Dirac sector and of the neutral Fermi surface, and then combining them in a controlled way to obtain the measurable σ_{ij} or ρ_{ij} .

To access the *d.c.* limit in the quantum critical fan, we then follow the strategy developed for the bandwidth-tuned Mott transition and related fractionalized QCPs [28, 38, 40]. We employ a large- N expansion in which the number of critical fermion flavors is generalized to N , while the Chern–Simons levels are simultaneously promoted to scale with N [42]. This choice keeps the Chern–Simons mixing at the same parametric order as the matter-induced polarizations, making the gauge structure explicit and controlled throughout the $1/N$ expansion. At $N = \infty$ the driven critical carriers are effectively collisionless, leading to an unphysical Drude-like $\delta(\omega)$ contribution (or a sharp peak) in the conductivity. This is precisely the artifact encountered in one-loop (collisionless) Kubo calculations: the absence of inelastic scattering prevents current relaxation and produces a singular low-frequency response.

The leading *physical* DC conductivity arises at $O(1/N)$, where scattering off the emergent gauge fluctuations broadens the spurious δ -function into a finite-width response. Concretely, we formulate a quantum Boltzmann equation (QBE) for the distribution functions of the critical Dirac quasiparticles and quasiholes in the presence of a weak, spatially uniform electric field at frequency ω , and compute the collision integral using the equilibrium spectral function of the relevant emergent gauge mode[37–39]. The resulting transport relaxation rate scales as

$$\frac{1}{\tau_{\text{tr}}} \sim \frac{T}{N} \times (\text{universal function}), \quad (1)$$

so that the DC conductivity is finite at leading nontrivial order in $1/N$ and exhibits the expected quantum critical

scaling. In this way, the Ioffe–Larkin composition rule provides the bridge from parton responses to the physical conductivity, while the large- N QBE supplies the controlled finite- T resummation of inelastic processes that removes the divergent low-frequency peak and yields a universal DC transport coefficient.

The paper is organized as follows. In Sec.IIA we briefly review the critical theory of the CFL-FL phase transition in the $\nu = -1/2$ case, and give a general picture of resistivity in the critical region. In Sec.IIB, we manifest the derivation of Ioffe–Larkin rule of this system by equations of motion. In Sec.III, we review the method of large- N expansion and give the low energy effective theory under this approximation. In Sec.IV, we studied the Transport data of this critical theory by quantum Boltzmann equation and show the result of DC resistivity. In Sec.V, we repeat the same process for the more complicated $\nu = -3/4$ case.

II. CFL TO FL TRANSITION IN MOIRÉ MATERIAL OF $\nu = -1/2$ CASE

A. Critical Theory of QED-Chern-Simons coupled to spinon Fermi surface

Motivated by recent observations of fractional quantum anomalous Hall (FQAH) states and composite Fermi liquid (CFL) phenomenology in moiré Chern bands, Ref. [26] develops effective field theories for unconventional phase transitions out of quantum Hall states upon tuning the bandwidth (e.g. by displacement field) at fixed filling. A central theme is that such transitions can be organized by separating the charge sector from the Fermi-surface sector using an emergent gauge structure: the quantum Hall/CFL physics is encoded in a strongly correlated charge sector, while gapless metallic behavior can persist in a neutral sector coupled to gauge fluctuations.

In particular, for the CFL to FL transition at $\nu = \frac{1}{2}$, the critical theory is constructed by combining (i) a critical theory for a bosonic Laughlin–superfluid transition at $1/2$ filling and (ii) a neutral Fermi surface, glued together by an emergent gauge field and Chern–Simons terms.

Here c denotes the low-energy annihilation operator of the physical electron in the (valley-polarized) partially filled $C = 1$ moiré Chern band, and A is the external probe gauge field that couples to the conserved electric charge. Here we use the parton construction $c = \Phi f$, with an emergent internal $U(1)$ gauge field $a_\mu = (a_0, \mathbf{a})$ enforcing the gauge redundancy $\Phi \rightarrow e^{i\theta}\Phi$, $f \rightarrow e^{-i\theta}f$. We assign the physical electromagnetic charge to Φ , so the charge sector couples to $A + a$, while f is electrically neutral and forms a Fermi surface described by \mathcal{L}_f .

For the CFL to FL transition at $\nu = \frac{1}{2}$, the charge-sector transition can be formulated as a bosonic Laughlin–superfluid transition at effective filling $\nu_\Phi = \frac{1}{2}$ (the electronic CFL corresponds to Φ in a Laughlin state,

while the FL corresponds to Φ condensed). A convenient critical description of this bosonic transition uses a further fermionic partonization of the boson,

$$\Phi = f_1 f_2,$$

which introduces additional emergent gauge constraints. In the mean-field construction of Ref. [26], tuning band parameters drives a Chern-number-changing transition in the f_2 sector. At low energies this becomes a Dirac theories coupled to emergent gauge fields b , giving the critical Lagrangian [26]:

$$\mathcal{L}_{\text{critical}} = \mathcal{L}_\psi + \mathcal{L}_f + \mathcal{L}_{\psi f}, \quad (2)$$

$$\begin{aligned} \mathcal{L}_\psi &= -i\bar{\psi}(\partial - i\psi)\psi + M\bar{\psi}\psi, \\ \mathcal{L}_f &= f^\dagger \left[i\partial_t + ia_0 + \mu + \frac{1}{2m}(\nabla + i\mathbf{a})^2 \right] f, \\ \mathcal{L}_{CS} &= \frac{1}{4\pi}(b + a + A)d(b + a + A) - \frac{1}{4\pi}bdb \end{aligned} \quad (3)$$

The Dirac mass M is the tuning parameter that drives the transition: changing the sign of M changes the induced Chern–Simons response of the ψ sector, so that after integrating out gapped modes one obtains either (i) the Φ -Laughlin state (corresponding to the electronic CFL) or (ii) the Φ superfluid (corresponding to the electronic FL via Higgsing of a_μ).

The relation between Φ and the Dirac fields ψ is indirect: ψ arise as the continuum Dirac fermions describing the Chern-number-changing band touchings of the auxiliary fermionic partons in the decomposition $\Phi = f_1 f_2$. The physical boson operator Φ itself is not a simple bilinear in ψ ; rather, it corresponds to a gauge-invariant monopole operator of the emergent gauge fields in the critical theory (schematically a monopole that inserts the appropriate 2π flux and is dressed by fermion zero-modes to be gauge neutral), and it carries unit charge under the background/probe field A through the BF coupling in \mathcal{L}_{CS} .

As the critical point represents a scale-invariant theory, the physical observables follow universal scaling behaviors. The compressibility $\frac{dn}{d\mu}$ behaves linear in T since total charge is a conserved quantity and there is a protected scaling dimension associated with charge density. The electrical resistivity tensor also follows a universal scaling form, i.e.

$$\rho_{ij} - \rho_{ij;m} = \frac{h}{e^2} \mathcal{R}_{ij} \left(\frac{\omega}{T}, \frac{\delta}{T^{\frac{1}{\nu_z}}} \right), \quad (4)$$

where ν, z are the correlation length exponent and dynamical exponent and δ the tuning parameter (i.e. displacement field) that controls the transition, and $\rho_{ij;m}$ the resistivity tensor measured on the metal side. The following calculation will find the universal scaling function \mathcal{R}_{ij} (fig 1) at $\delta = 0$, as a function of ω/T .

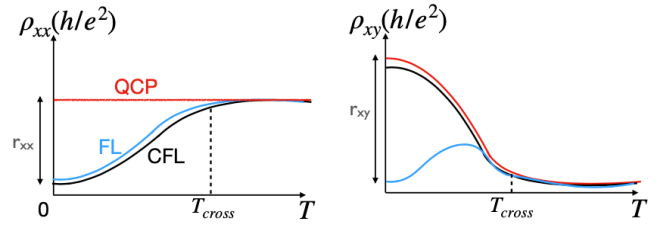


FIG. 1: (Adapted from Ref. [26]) The resistivity as a function of temperature. The blue curves are for the FL, the black for the CFL, and the red for the quantum critical points. We compute the universal jump r_{xx}, r_{xy} in the quantum critical regime ($T \sim 0$), which are of order h/e^2 .

B. Resistivity in the critical regime

The electromagnetic response of the physical electrons can be organized using the standard Ioffe–Larkin composition rule in terms of the parton responses[41]. The key point is that the external probe field A couples to gauge-invariant combinations of internal gauge and matter fields, and after integrating out the matter fields the remaining effective action becomes quadratic in the gauge fluctuations. In this regime the full linear response can be obtained exactly by solving the Gaussian theory.

Integrating out the fermions renormalizes the gauge-field sector and yields the quadratic Euclidean action

$$\begin{aligned} \mathcal{S}_E[b, a; A] &= \frac{1}{2} \int_{\mathbf{p}, \omega} b_\mu^* \Pi_\psi^{\mu\nu} b_\nu + a_\mu^* \Pi_f^{\mu\nu} a_\nu - b_\mu^* \Pi_{CS}^{\mu\nu} b_\nu \\ &\quad + (b_\mu + a_\mu + A_\mu)^* \Pi_{CS}^{\mu\nu} (b_\nu + a_\nu + A_\nu). \end{aligned} \quad (5)$$

Here Π_ψ and Π_f are the polarization tensors generated by integrating out ψ and f , respectively, while $\Pi_{CS}^{\mu\nu} = \frac{i}{2\pi} \epsilon_{\mu\nu\rho} P_\rho$ encodes the Chern–Simons response. All gauge fields are involved in terms of their Fourier components, i.e., $x(\mathbf{p}, \omega) = x^*(-\mathbf{p}, -\omega)$. Since the theory is quadratic, the linear electromagnetic response is fully determined by the saddle-point (equations of motion) for b, a in the presence of A .

The physical current is obtained by varying the action with respect to the external probe field A ,

$$J_\mu^{\text{phy}} = \frac{\delta \mathcal{S}_E}{\delta A_\mu} = \Pi_{\mu\nu}^{\text{phy}} A_\nu = \Pi_{CS}^{\mu\nu} (b_\nu + a_\nu + A_\nu),$$

which defines the physical electromagnetic polarization Π_A^{phy} . To determine Π_A^{phy} , we solve the equations of motion implied by \mathcal{S}_E :

$$\begin{cases} \frac{\delta \mathcal{S}_E}{\delta b_\mu} = \Pi_\psi^{\mu\nu} b_\nu + \Pi_{CS}^{\mu\nu} (a_\nu + A_\nu) = 0 \\ \frac{\delta \mathcal{S}_E}{\delta a_\mu} = \Pi_f^{\mu\nu} a_\nu + \Pi_{CS}^{\mu\nu} (b_\nu + a_\nu + A_\nu) = 0 \end{cases} \quad (6)$$

These linear constraints express the internal gauge fields in terms of the external source A . Eliminating b and a

then gives an effective response purely for A , equivalently Π_A^{phy} . Solving the above system yields

$$(\Pi^{\text{phy}})^{-1} = \Pi_{CS}^{-1} + \Pi_f^{-1} + (\Pi_\psi - \Pi_{CS})^{-1} \quad (7)$$

which is the Ioffe–Larkin-type composition rule written at the level of polarization tensors. The inverse structure reflects the fact that, once the internal gauge constraints are imposed, the corresponding resistive channels add in series.

Applying the Kubo formula,

$$\rho(\omega)^{-1} = \sigma(\omega) = \lim_{\mathbf{p} \rightarrow 0} \frac{1}{i\omega} \Pi(\omega, \mathbf{p}),$$

and substituting $\rho_{CS,xy} = -\rho_{CS,yx} = 2\pi$ then yields the Ioffe–Larkin rule for this system:

$$\rho_{ij}^{\text{phy}} = \left(\rho_f + \frac{4\pi^2 \rho_\psi}{4\pi^2 + \rho_\psi^2} \right) \delta_{ij} - \frac{8\pi^3}{4\pi^2 + \rho_\psi^2} \epsilon_{ij}, \quad (8)$$

which makes the “series connection” structure transparent: the longitudinal resistivities add, while the Chern–Simons sector generates the antisymmetric (Hall) component encoded by ϵ_{ij} . The ρ_ψ in the denominator comes from the inversion of the combination of Hall and longitude conductivity.

Across the critical point, ρ_f exhibits smooth behaviour. Therefore, the resistivity in the critical regime is controlled by the ψ sector. In the DC limit ($q = 0, \omega \rightarrow 0$), it gives a universal jump at the critical point [26], whose low-energy dynamics is dominated by scattering off the emergent gauge mode b . Physically, the jump is therefore set by the relaxation of this gauge fluctuation, as encoded in the imaginary part of its effective propagator,

$$D_b = \text{Im}(1/\Pi_{b,\text{eff}}).$$

In our setup, b does not couple directly to the spinon Fermi surface. Instead, it is coupled to an intermediate gauge field a through a Chern–Simons (CS) term, while a itself couples minimally to the spinon Fermi surface f . Landau damping refers to the fact that in the presence of coupling to $U(1)$ gauge fields, the scattering process of matter fields with non-zero finite frequency exchange is heavily suppressed from the behavior of the self-energy. One might then expect Landau damping from the Fermi surface to be transmitted to b . A key result of our theory is that this does not occur, and the reason is ultimately kinematic, rooted in the structure of the CS interaction.

We will not show explicit illustration here (interested readers can find details in App.A). However, This result has a simple physical interpretation. The CS propagator is purely antisymmetric and proportional to momentum, so it vanishes in the infrared. As a result, it necessarily mixes longitudinal and transverse components of the gauge field and suppresses their low-energy weight. By contrast, Landau damping from a Fermi surface resides

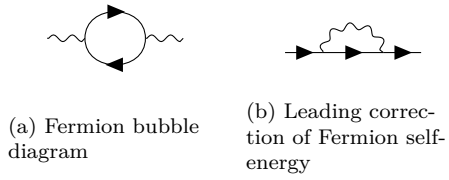


FIG. 2: The leading terms of 1-loop diagram where straight line is Dirac ψ Fermion and wavy line is gauge b boson. Wavy lines represent gauge propagator while solid lines represent free propagator of Dirac fermions. Diagram (a) is of order N since each flavor can form a loop, while diagram (b) is of order N^{-1} and thus suppressed

entirely in the transverse sector. The CS-induced mixing, together with its infrared suppression, therefore washes out the damping channel. In this sense, the CS structure acts as a filter: although the gauge field a is strongly damped by the spinon Fermi surface, this damping cannot be efficiently transmitted to b .

III. PERTURBATION THEORY UNDER LARGE-N LIMIT

A. Large-N expansion

To extract the leading correction to the fermion conductivity, we employ a large- N expansion. We generalize the fermions to N flavors and simultaneously promote the levels of the Chern–Simons terms to N . This choice keeps the Chern–Simons contributions at the same parametric order as the matter-induced polarization effects, so that their impact remains explicit throughout the $1/N$ expansion. The corresponding imaginary-time Lagrangian with the absence of external field A is

$$\mathcal{L}_N = \sum_{l=1}^N (\mathcal{L}_{\psi,l} + \mathcal{L}_{f,l}) + \frac{iN}{4\pi} ada + \frac{iN}{2\pi} bda, \quad (9)$$

with

$$\mathcal{L}_{\psi,l} = -\bar{\psi}_l (\partial - i\psi) \psi_l - M \bar{\psi}_l \psi_l, \quad (10)$$

$$\mathcal{L}_{f,l} = f_l^\dagger \left[\partial_\tau - ia_0 - \mu - \frac{1}{2m} (\nabla + i\mathbf{a})^2 \right] f_l. \quad (11)$$

Here we adopt the Euclidean γ matrices $\gamma^0 = \sigma^z, \gamma^1 = -\sigma^y, \gamma^2 = \sigma^x$, so that $\bar{\psi} \gamma^i \psi = i \psi^\dagger \sigma^i \psi$.

Working in the Lorentz gauge, the free propagators can be directly read off from \mathcal{L}_N :

$$D_a(P) = \left(\frac{N}{2\pi} \epsilon_{\mu\nu\lambda} P_\lambda - \frac{1}{\epsilon} P_\mu P_\nu \right)^{-1} \equiv (NP')^{-1},$$

$$D_\psi(P) = \frac{1}{i\mathcal{P} + M},$$

$$D_f(P) = \left(-i\omega_n + \frac{\mathbf{p}^2}{2m} - \mu \right)^{-1} \equiv G_P,$$

In the large- N expansion, N plays a role analogous to $1/\hbar$: diagrams organize according to their powers of

$1/N$. In particular, among all one-particle-irreducible (1PI) contributions to the full gauge polarization function, the leading term is given by the fermion bubble, while all other 1PI corrections are suppressed by additional negative powers of N (see Fig.2a).

For fermion self-energy diagrams, the leading correction is of N^{-1} order (see Fig.2b). We therefore neglect the mass renormalization and set $M(T) = 0$ at the critical point, consistent with the leading large- N treatment.

The 1-loop bubble diagrams of ψ and f read:

$$\Pi_\psi^{\mu\nu}(P \equiv (\nu_l, \mathbf{p})) = -T \sum_{\omega_n} \int \frac{d^2\mathbf{k}}{(2\pi)^2} \frac{2\{2K^{(\mu}(K+P)^{\nu)} - [\mathbf{k} \cdot (\mathbf{k} + \mathbf{p}) + \omega_n(\omega_n + \nu_l)]\delta^{\mu\nu}\}}{(\epsilon_{\mathbf{k}}^2 + \omega_n^2) [\epsilon_{\mathbf{k}+\mathbf{p}}^2 + (\omega_n + \nu_l)^2]}, \quad (12)$$

$$\Pi_f^{ij}(P \equiv (\nu_l, \mathbf{p})) = T \sum_{\omega_n} \int \frac{d^2\mathbf{k}}{(2\pi)^2} \left(\frac{\delta^{ij}}{m} G_K + \frac{1}{m^2} (k - p/2)^i (k - p/2)^j G_K G_{K-P} \right), \quad (13)$$

$$\Pi_f^{00}(P \equiv (\nu_l, \mathbf{p})) = T \sum_{\omega_n} \int \frac{d^2\mathbf{k}}{(2\pi)^2} G_K G_{K-P}. \quad (14)$$

The polarization bubble Π_ψ also yields the leading contribution to σ_ψ , which has been known in [38]. To zeroth order in $1/N$, one finds

$$\sigma_\psi = \sigma_{qp} + \sigma_{coh}, \quad (15)$$

$$\sigma_{qp}(\omega) = \frac{\ln 2}{2} \left[\delta\left(\frac{\omega}{T}\right) + i\mathcal{P}\left(\frac{T}{\omega}\right) \right], \quad (16)$$

$$\text{Re}[\sigma_{coh}(\omega)] = \frac{1}{16} \tanh \frac{|\omega|}{4T}. \quad (17)$$

In particular, for $\omega \gg T$ the conductivity σ_ψ approaches a constant $1/16$. However for $\omega < T$ this formula presents a nonphysical singularity peak, which implies that the correct conductivity is beyond first order perturbation and may contain infinite orders of diagrams. We will discuss and cure this by hydrodynamic method in Sec.IV. Before that we should first grasp the low-energy spectrum of gauge boson that interacts with ψ .

B. Low energy effective theory

To study the low-energy property of b boson, we integrate out all other fields to obtain an effective action quadratic in the external gauge field b , which read as

$$S_{\text{eff}}[b] = \frac{N}{2} \int \frac{d^3P}{(2\pi)^3} b_\mu(-P) \cdot \Pi_b^{\mu\nu}(P) \cdot b_\nu(P), \quad (18)$$

where the polarization function $\Pi_b(P)$ is identified with the inverse of $-\Delta_b$, i.e. the full (dressed) propagator

of b . In the large- N expansion adopted here, Π_b can be expressed in terms of the response tensors Π_ψ and Π_f generated by the ψ and f sectors, together with the Chern-Simons mixing encoded in the gauge-field structure, following directly from the Feynman rules.

To calculate Π_b , we first write down the inverse full propagator equations based on Feynman rules:

$$\begin{cases} \Delta_a^{-1} = -NP' - N\Pi_f \\ N\Pi_b = -\Delta_b^{-1} = N\Pi_\psi + N^2 P \cdot \Delta_a \cdot P \end{cases}, \quad (19)$$

where Δ s denote the corresponding propagators.

Solving the above equation set yields the tensor Π_b . To decouple the temporal component and spacial component of gauge field b , it's much simpler to work under Coulomb gauge in which $\nabla \cdot \mathbf{b} = 0$, and thus the spacial component of gauge field can be simplified to a scalar: $\mathbf{b}(\mathbf{q}) = (\hat{z} \times \hat{q})b(\mathbf{q})$. The effective action turns into

$$S_b = N \int_{\Omega_n, \mathbf{q}} \frac{q^2}{\Omega_n^2 + q^2} |b_0|^2 \Pi_{b,L}(\Omega_n, q) + |b|^2 \Pi_{b,T}(\Omega_n, q) + \frac{q}{\sqrt{\Omega_n^2 + q^2}} (b_0^* b - b^* b_0) \Pi_{b,O}(\Omega_n, q), \quad (20)$$

where the projective components $\Pi_{T,L,O}$ corresponding to transverse, longitudinal and antisymmetric sectors of the polarization functions respectively and their exact definition and calculation can be found in App.A. The last term mixes b_0 and the transverse spatial mode b

through the parity-odd response $\Pi_{b,O}$, and the prefactor $q/\sqrt{\Omega^2 + q^2}$ originates from projecting $P_O^{\mu\nu}$ onto the Coulomb-gauge basis.

Further integrate out b_0 , we obtain

$$\mathcal{S}_b = N \int_{\Omega, \mathbf{q}} |b|^2 (\Pi_{b,T} + \Pi_{b,O}^2 / \Pi_{b,L}). \quad (21)$$

We denote the factor of $|b|^2$ in effective action by $\Pi_{b,\text{eff}}$, i.e.,

$$\Pi_{b,\text{eff}} := \Pi_{b,T} + \Pi_{b,O}^2 / \Pi_{b,L}. \quad (22)$$

which is the effective transverse polarization that directly determines the propagator of the spatial gauge mode b in Coulomb gauge, and therefore controls the spectral function entering the collision integral and the transport relaxation rate in the QBE analysis. The calculation of $\Pi_{b,\text{eff}}$ can be found in App. A. It is given that

$$\Pi_{b,\text{eff}} \simeq \Pi_{\psi,T} \quad (23)$$

in $\nu = -1/2$ case.

IV. CRITICAL TRANSPORT NEAR THE CFL TO FL TRANSITION

Our goal is to obtain the *universal* low-frequency transport in the quantum critical (QC) regime of the CFL–FL transition. A key lesson from earlier analyses of QC transport is that the order of limits $\omega \rightarrow 0$ and $T \rightarrow 0$ does *not* commute, and therefore a strictly $T = 0$ Kubo calculation generally captures only the collisionless, high-frequency response rather than the DC conductivity.

In particular, Damle and Sachdev[38] emphasized that the conductivity at a (2+1)-dimensional interacting QCP takes the scaling form

$$\sigma(\omega, T) = \frac{e^2}{\hbar} \Sigma\left(\frac{\hbar\omega}{k_B T}\right), \quad (24)$$

but the limiting regimes have distinct physical content: for $\hbar\omega \gg k_B T$ the response is dominated by *phase-coherent* motion of excitations created by the external field, while the DC limit $\hbar\omega \ll k_B T$ is governed by *incoherent, inelastic* scattering among *thermally excited* carriers and relaxation to local equilibrium. As shown explicitly for fractional quantum Hall critical points in [38], a calculation performed strictly at $T = 0$ determines $\Sigma(\infty)$, whereas the DC conductivity is controlled by $\Sigma(0)$ and requires a finite- T treatment of collisions. The appropriate framework in this hydrodynamic regime is a quantum kinetic equation: one first formulates the transport problem at $T > 0$ and small ω , and then takes the DC limit.

A closely related message arises in the slave-rotor theory of the bandwidth-tuned Mott transition[40]: at $N = \infty$ the critical charge sector is effectively collisionless and

produces a Drude $\delta(\omega)$ contribution, while the universal DC resistivity (or conductivity) appears only after including the leading $1/N$ scattering processes. There, the quantum Boltzmann equation provides a controlled way to resum the leading collision processes and broaden the spurious δ -function into a finite-width peak, yielding a finite and universal DC transport coefficient.

The same logic applies here. In our large- N formulation, we can assign the charge to one single flavour of the critical Dirac parton ψ . In this way, only one flavor is directly driven by the external electric field, while the remaining $N - 1$ flavors stay near equilibrium and act as an effective bath. This makes the QBE particularly natural and controlled: the collision integral is $O(1/N)$ (because the relevant gauge propagator is $O(1/N)$), so the transport relaxation rate scales as

$$\frac{1}{\tau_{\text{tr}}} \sim \frac{T}{N} \times (\text{universal function}), \quad (25)$$

and the resulting DC conductivity is finite at leading nontrivial order in $1/N$. Moreover, the gauge sector produces prominent low-energy scattering channels in the QC regime, whose impact is *precisely* what is missed by a purely collisionless ($T = 0$) computation. Therefore, to correctly capture the DC transport and its universal scaling function in the QC fan, we employ a quantum Boltzmann equation for the distribution functions of ψ quasiparticles and quasiholes, and solve it to leading order in $1/N$.

A. Quantum Boltzmann Equation

To formulate the QBE, we apply an external spatially uniform oscillating electric field $\mathbf{E}(t)$ with frequency ω . The DC conductivity is obtained by first taking $\omega \rightarrow 0$, and then taking the low-temperature limit while keeping $O(\omega/T) = O(1)$. This order of limits is important: it allows the transport calculation to remain sensitive to gauge fluctuations that are parametrically soft near $T \rightarrow 0$.

In the large- N limit, there are N identical copies of ψ . We assign an electric charge to a single flavor ψ_1 so that it couples directly to the oscillating electric field $\mathbf{E}(t)$. The transport response is then mediated by ψ_1 , and the DC conductivity is controlled by the collisions between ψ_1 and the emergent gauge field b .

The standard mode expansion of ψ_1 reads:

$$\psi_1(x, t) = \int_{\mathbf{k}} \left[\gamma_+(\mathbf{k}, t) \left(\frac{\frac{1}{\sqrt{2}}}{\frac{\mathbf{k}}{\sqrt{2}}} \right) + \gamma_-(\mathbf{k}, t) \left(\frac{\frac{1}{\sqrt{2}}}{-\frac{\mathbf{k}}{\sqrt{2}}} \right) \right] e^{i\mathbf{k} \cdot \mathbf{x}} \quad (26)$$

Where $\tilde{k} = (k_x + ik_y)/|\mathbf{k}|$. We identify γ_+^\dagger and γ_-^\dagger as creation operator of quasiparticles and quasiholes respectively since γ_+^\dagger and γ_-^\dagger generates opposite energy. (γ_+^\dagger is the positive one.)

Using this expansion, we can express the electric current $J_i = \bar{\psi}_1 \gamma_i \psi_1$ in terms of γ_\pm . The expectation

value of the current can be decomposed into two parts: $\mathbf{J} = \mathbf{J}_I + \mathbf{J}_{II}$, where

$$\begin{aligned}\mathbf{J}_I(t) &= \sum_{s=\pm} \int_{\mathbf{k}} \frac{s\mathbf{k}}{\epsilon_{\mathbf{k}}} \langle \gamma_s^{\dagger}(\mathbf{k}, t) \gamma_s(\mathbf{k}, t) \rangle \\ &\equiv \int_{\mathbf{k}} V \frac{\mathbf{k}}{\epsilon_{\mathbf{k}}} (f_+(\mathbf{k}, t) - f_-(\mathbf{k}, t)),\end{aligned}\quad (27)$$

$$\mathbf{J}_{II} = - \int_{\mathbf{k}} \frac{(\hat{\mathbf{z}} \times \mathbf{k})}{|\mathbf{k}|} \left(\gamma_+^{\dagger}(\mathbf{k}) \gamma_-(-\mathbf{k}) - \gamma_-^{\dagger}(\mathbf{k}) \gamma_+(\mathbf{k}) \right). \quad (28)$$

V is the volume of the whole system. In equilibrium and in the absence of external perturbations, the distribution

functions reduce to the Fermi functions

$$f_{\pm}(\mathbf{k}, t)_0 = n_F(\pm \epsilon_{\mathbf{k}}) = \frac{1}{e^{\pm \beta \epsilon_{\mathbf{k}}} + 1}, \epsilon_{\mathbf{k}} = |\mathbf{k}|. \quad (29)$$

Physically, \mathbf{J}_I is the conventional transport current carried by quasiparticles and quasiholes, which contribute with opposite signs due to their opposite charges. The term \mathbf{J}_{II} corresponds to an interband (pair-production) contribution that is suppressed in the low-frequency transport regime considered here; accordingly, we will work in the approximation $\mathbf{J}_{II} = 0$.

Applying Fermi's golden rule, the collision term can be written as $I_b \sim \frac{\text{collision cases}}{\text{relaxation time of } b}$:

$$\begin{aligned}(\partial_t + s\mathbf{E} \cdot \partial_{\mathbf{k}}) f_s(\mathbf{k}, t) &= I_b [f_{\pm}] \\ &= - \frac{1}{N} \int_0^{\infty} \frac{d\Omega}{\pi} \int \frac{d^2 q}{(2\pi)^2} (\mathbf{k} \times \hat{\mathbf{q}})^2 D_b(\Omega, q) \\ &\quad \times \left\{ \frac{(2\pi)\delta(\epsilon_{\mathbf{k}} - \epsilon_{\mathbf{k}+q} - \Omega)}{4\epsilon_{\mathbf{k}}\epsilon_{\mathbf{k}+q}} \left[f_s(\mathbf{k}, t)(1 - f_s(\mathbf{k} + \mathbf{q}, t))(1 + n(\Omega)) - f_s(\mathbf{k} + \mathbf{q}, t)(1 - f_s(\mathbf{k}, t))n(\Omega) \right] \right. \\ &\quad + \frac{(2\pi)\delta(\epsilon_{\mathbf{k}} - \epsilon_{\mathbf{k}+q} + \Omega)}{4\epsilon_{\mathbf{k}}\epsilon_{\mathbf{k}+q}} \left[f_s(\mathbf{k}, t)(1 - f_s(\mathbf{k} + \mathbf{q}, t))n(\Omega) - f_s(\mathbf{k} + \mathbf{q}, t)(1 - f_s(\mathbf{k}, t))(1 + n(\Omega)) \right] \\ &\quad \left. + \frac{(2\pi)\delta(\epsilon_{\mathbf{k}} + \epsilon_{\mathbf{k}-q} - \Omega)}{4\epsilon_{\mathbf{k}}\epsilon_{\mathbf{k}-q}} \left[f_s(\mathbf{k}, t)(1 - f_{-s}(\mathbf{k} - \mathbf{q}, t))(1 + n(\Omega)) - (1 - f_s(\mathbf{k}, t))f_{-s}(-\mathbf{k} + \mathbf{q}, t)n(\Omega) \right] \right\}\end{aligned}\quad (31)$$

where the propagator $D_b(\Omega, p) = \text{Im}[1/\Pi_{b,\text{eff}}(\Omega, p)] \simeq \text{Im}[1/\Pi_{\psi,T}(\Omega, p)]$ enters into the QBE via its spectral functions, which dictate the density of states the Dirac fermion excitations can scatter into. They are evaluated in equilibrium. This is justified in the large- N limit since the external field couples to a single Dirac flavor such that the associated nonequilibrium corrections to the polarization functions sublead in $1/N$. In other words, the Dirac flavors that do not directly couple to the electric field $\psi_{\alpha>1}$ play the role of an effective bath at equilibrium.

The scattering terms on the RHS all scale like $1/N$ fixed by the order of the gauge propagator. When $N \rightarrow \infty$, the scattering terms vanish and Dirac Fermions behave as free particles. The sharp peak singularity in Eq.16 is reproduced. At finite $1/N$, these collisions broaden the singular contribution, yielding a finite DC conductivity.

Suppose the system is near equilibrium, we expand the distribution function f_s to linear order in \mathbf{E} :

$$f_s(\mathbf{k}, \omega) = n_F(s\epsilon_{\mathbf{k}}) 2\pi\delta(\omega) + s\mathbf{E} \cdot \mathbf{k} \varphi(\mathbf{k}, \omega). \quad (32)$$

where we have Fourier transformed from time to frequency. The unknown function $\varphi(\mathbf{k}, \omega)$ parametrizes the anisotropic deformation of the distribution induced by \mathbf{E} .

The simplification of I_b is displayed in App.B. Putting them together we obtain the following linearized equation for $\varphi(p, \omega)$:

$$-i\omega\varphi(p, \omega) + g(p)/T^2 = \frac{T}{N} \left\{ -F_b(p)\varphi(p, \omega) + \int dp' K_b(p', p)\varphi(p', \omega) \right\} \quad (33)$$

where we have Fourier transformed from time to frequency and have introduced dimensionless variables p denoting the rescaled momentum: $p = k/T$. On the LHS, the inhomogeneous driving term is $g(p) = \partial_{\epsilon_p} n_F(\epsilon_p)/\epsilon_p = -e^{\epsilon_p}/\epsilon_p (e^{\epsilon_p} + 1)^2$, which originates from the linearized drift term $s\mathbf{E} \cdot \partial_{\mathbf{k}} f_s$ evaluated on the equilibrium distribution. On the RHS, $F_b(p)$ can be identified with the universal function of scattering rate in Eq.25, i.e.,

$$\frac{1}{\tau_{\text{tr}}} \sim \frac{T}{N} \times F_b(p), \quad (34)$$

This elastic scattering rate obtained in the static regime is universal in the sense that it does not depend on the Fermi-surface information. We have also introduced the dimensionless kernel $K_b(p', p)$ describing the inelastic

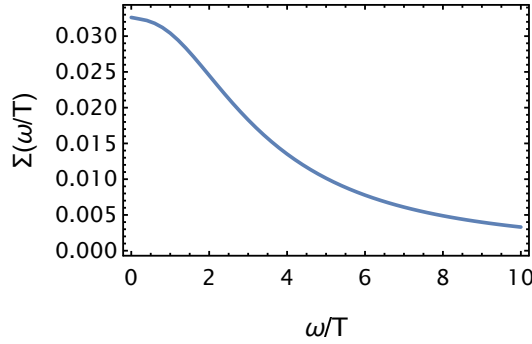


FIG. 3: Real part of the scaling function $\Sigma(\omega/T)$ of $\nu = -1/2$ case.

processes in which the Dirac Fermions exchange energy with the gauge b bosons.

B. Solution

In the low temperature limit $O(\omega/T) = O(1)$, we rescale the parameters to dimensionless: $\tilde{\omega} = \omega N/T$, $\Phi(p, \tilde{\omega}) = \frac{T^3}{N} \varphi(p, \omega)$. Eq.33 becomes:

$$-i\tilde{\omega}\Phi(p, \tilde{\omega}) + g(p) = -F_b(p)\Phi(p, \tilde{\omega}) + \int dp' K_b(p', p)\Phi(p', \tilde{\omega}) \quad (35)$$

Assuming the external \mathbf{E} field is in the x direction, the DC conductivity[40]:

$$\sigma_\psi(\omega) = \frac{\langle J_{Ix}(\omega) \rangle}{E_x(\omega)} = \frac{N}{2\pi} \int_0^{\Lambda/T} dp \frac{p^3 \Phi(p, \tilde{\omega})}{\epsilon_p} \quad (36)$$

In this case we have $N = 1$. Combining Eq.24,36, we show the real part of the scaling function in Fig.3. The DC conductivity reads as $\sigma_\psi(0) = \frac{e^2}{h} \times 0.033$.

V. CRITICAL TRANSPORT OF $\nu = -3/4$ CASE

Similar to Sec.IIA, for the CFL to FL transition at $\nu = -\frac{3}{4}$ (equivalently the $\nu_e = \frac{1}{4}$ problem after accounting for the $\nu = -1$ background), the critical theory is constructed by combining a critical theory for a bosonic Laughlin–superfluid transition and a neutral Fermi surface, glued together by an emergent gauge field and Chern–Simons terms. The only difference is that Φ has effective filling $\nu_\Phi = \frac{1}{4}$, with further partitionization:

$$\Phi = f_1 f_2 f_3 f_4,$$

which introduces additional emergent gauge constraints. In the mean-field construction of Ref. [26], tuning band parameters drives a Chern-number-changing transition in the f_3, f_4 sector. At low energies this becomes two Dirac theories (four Dirac cones total) coupled to emergent gauge fields b_i , giving the critical Lagrangian [26]:

$$\mathcal{L}_{critical} = \mathcal{L}_\psi + \mathcal{L}_f + \mathcal{L}_{\psi f}, \quad (37)$$

with the constituent lagrangian

$$\begin{aligned} \mathcal{L}_\psi &= \sum_{i=1}^2 i\bar{\psi}_i (\partial\tau_0 - i\psi_i \tau_0) \psi_i + M\bar{\psi}_i \psi_i, \\ \mathcal{L}_f &= f^\dagger \left[i\partial_t + ia_0 + \mu + \frac{1}{2m}(\nabla + i\mathbf{a})^2 \right] f, \\ \mathcal{L}_{CS} &= \frac{1}{2\pi} (A + a + b_1 + b_2) d\alpha - \frac{2}{4\pi} \alpha d\alpha - \sum_{i=1,2} \frac{1}{4\pi} b_i db_i, \end{aligned} \quad (38)$$

where each Dirac fermion carry two flavors transformed in the τ space, so in total there are 4 flavors of Dirac fermions.

This represents an interesting field theory where translations interchange the Dirac fermion flavors. Integrating out the fermions renormalizes the gauge-field sector and yields the quadratic Euclidean action

$$\begin{aligned} \mathcal{S}_E[b_i, a, \alpha; A] &= \frac{1}{2} \int \sum_{i=1,2} b_{i\mu}^* \left(\Pi_{\psi_i}^{\mu\nu} - \Pi_{CS}^{\mu\nu} \right) b_{i\nu} \\ &+ a_\mu^* \Pi_f^{\mu\nu} a_\nu - 2a_\mu^* \Pi_{CS}^{\mu\nu} \alpha + 2(A_\mu + a_\mu + b_{i\mu})^* \Pi_{CS}^{\mu\nu} \alpha_\nu. \end{aligned} \quad (39)$$

Analogous to Eq.6, we can write the equations of motion for this system:

$$\begin{cases} \frac{\delta \mathcal{S}_E}{\delta b_{i\mu}} = (\Pi_{\psi_i}^{\mu\nu} - \Pi_{CS}^{\mu\nu}) b_{i\nu} + \Pi_{CS} \alpha_\nu = 0 \\ \frac{\delta \mathcal{S}_E}{\delta a_\mu} = \Pi_f^{\mu\nu} a_\nu + \Pi_{CS}^{\mu\nu} \alpha_\nu = 0 \\ \frac{\delta \mathcal{S}_E}{\delta \alpha_\mu} = -2\Pi_{CS}^{\mu\nu} \alpha_\nu + \Pi_{CS}^{\mu\nu} (A_\nu + a_\nu + b_{1\nu} + b_{2\nu}) = 0 \end{cases} \quad (40)$$

Solving these equations yields

$$(\Pi^{phy})^{-1} = 2\Pi_{CS}^{-1} + \Pi_f^{-1} + (\Pi_{\psi_1} - \Pi_{CS})^{-1} + (\Pi_{\psi_2} - \Pi_{CS})^{-1}, \quad (41)$$

and the Ioffe–Larkin rule for this system:

$$\rho_{ij}^{phy} = \left(\rho_f + \frac{8\pi^2 \rho_\psi}{4\pi^2 + \rho_\psi^2} \right) \delta_{ij} - \frac{16\pi^3}{4\pi^2 + \rho_\psi^2} \epsilon_{ij}, \quad (42)$$

Note that this equation closely resemble Eq.42, except a factor on the numerators, Thus our illustration in Sec.IIB still works for this case.

A. Effective propagator

In the large- N limit, the corresponding imaginary-time Lagrangian is

$$\begin{aligned} \mathcal{L}_N &= \sum_{l=1}^N (\mathcal{L}_{\psi,l} + \mathcal{L}_{f,l}) + \frac{iN}{2\pi} (a + b_1 + b_2) d\alpha \\ &- \frac{2iN}{4\pi} \alpha d\alpha - \sum_{i=1}^2 \frac{iN}{4\pi} b_i db_i, \end{aligned} \quad (43)$$

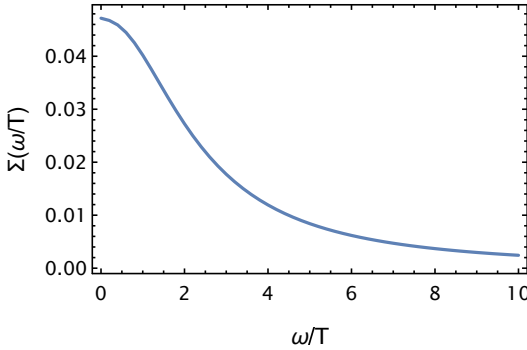


FIG. 4: Real part of the scaling function of $\nu = -3/4$ case.

with

$$\mathcal{L}_{\psi,l} = \sum_{i=1,2} -\overline{\psi_{i,l}}(\not{\partial} - i\not{b}_i)\psi_{i,l} - M\overline{\psi_{i,l}}\psi_{i,l}, \quad (44)$$

$$\mathcal{L}_{f,l} = f_l^\dagger \left[\partial_\tau - ia_0 - \mu - \frac{1}{2m}(\nabla + ia)^2 \right] f_l, \quad (45)$$

where the flavor is extended from 2 to $2N$, adopting the Euclidean γ matrices $\gamma^0 = \sigma^z, \gamma^1 = -\sigma^y, \gamma^2 = \sigma^x$, so that $\overline{\psi}\gamma^i\psi = i\psi^\dagger\sigma^i\psi$.

Utilizing the same method as which in Sec. III B, we can write down the propagator equations by order:

$$\begin{cases} \Delta_{b_2}^{-1} = -NP' - N\Pi_\psi, & \Delta_a^{-1} = -N\Pi_f \\ \Delta_\alpha^{-1} = -2NP' - N^2P \cdot \Delta_{b_2} \cdot P - N^2P \cdot \Delta_a \cdot P \\ N\Pi_b = -\Delta_{b_1}^{-1} = NP' + N\Pi_\psi + N^2P \cdot \Delta_\alpha \cdot P \end{cases} \quad (46)$$

where Δ s denote the propagators of corresponding gauge fields, while Π_ψ and Π_f are exact the same as $\nu = 1/2$ case given by Eq. 12, 13, 14. These equations, when treated as a system, is only meaningful for a single variable, Π_b , i.e., it will not give real full propagators for other gauge fields. (see App. A for explanations)

B. Quantum Boltzmann Equation

The form of QBE for $\nu = -3/4$ case is exactly the same as previous one in Eq. 33. But with a more complicated effective gauge propagator:

$$D_b(\omega, p) = \text{Im} \left\{ \frac{(q^2 - \omega^2 + 8\pi^2\Pi_{\psi,T}\Pi_{\psi,L})}{\Pi_{\psi,T}[2(q^2 - \omega^2) + 8\pi^2\Pi_{\psi,T}\Pi_{\psi,L}]} \right\}, \quad (47)$$

Again, $\Pi_{\psi,T}$ and $\Pi_{\psi,L}$ denote the transverse and longitude sector of the bubble diagram Π_ψ respectively. Replacing D_b in Eq. 30 by above expression yields the correct form of QBE core for $\nu = -3/4$ case.

Similarly, we can get the real part of the scaling function (Fig. 4). The DC conductivity reads as $\sigma_\psi(0) = \frac{e^2}{h} \times 0.047$.

VI. DISCUSSION

A. Conductivity at large frequencies

The DC conductivities calculated in Sec. IV and V correspond to the hydrodynamic limit, $\hbar\omega \ll k_B T$, where inelastic scattering among critical excitations dominates. In this regime, the system behaves as an incoherent thermal fluid. However, for $\hbar\omega \gg k_B T$, the system enters a collisionless regime where transport is governed by the coherent creation of particle-hole pairs. In this optical limit, the longitude conductivity approaches a different universal value for both cases[37]:

$$\sigma_\psi(\omega \gg T) \approx \frac{N}{16} \frac{e^2}{h}. \quad (48)$$

The full response function $\sigma(\omega/T)$ thus encodes a universal crossover between these two limits. Given that the physical resistivity is the sum of the critical sector ρ_ψ and the spectator Fermi surface ρ_f , the critical sector acts as a robust series resistor. This ensures that the crossover in σ_ψ should be observable as a frequency-dependent modulation of the total resistivity ρ_{xx} .

B. Thermal conductivity

According to the Ioffe-Larkin composition rule, the total thermal conductivity receives additive contributions from the Dirac fermion (ψ) and spinon (f) sectors,

$$\kappa = \kappa_\psi + \kappa_f, \quad (49)$$

i.e., it follows the parallel addition rule.

We first discuss the thermal conductivity associated with the Dirac fermions, denoted by κ_ψ . In the absence of the emergent b gauge field, the Dirac sector is described at low energies by a relativistic critical theory (a $(2+1)$ -dimensional CFT). In such a scale-invariant, translation-invariant setting, the heat current has a non-decaying overlap with conserved quantities, and the corresponding thermal transport contains a ballistic component. Equivalently, the frequency-dependent thermal conductivity exhibits a Drude weight,

$$\bar{\kappa}_\psi(\omega) = 2\pi D_T T \delta(\omega) + \bar{\kappa}_\psi^{\text{reg}}(\omega),$$

so that the dc limit of $\bar{\kappa}_\psi$ is formally divergent.

In our problem this idealized behavior is avoided once the Dirac fermions are coupled to the emergent b gauge field. Even though the bare b field is nondissipative, self-energy corrections generated by the Dirac matter produce a dissipative term in the gauge-field dynamics. This dissipation breaks the strict conformal/relativistic structure of the decoupled CFT and provides an efficient channel for relaxing the heat current. As a result, the dc thermal conductivity becomes finite in the quantum-critical regime and is fixed by scaling. In particular, up to a

dimensionless constant K_ψ set by the interacting fixed point,

$$\kappa_\psi = \frac{k_B^2}{\hbar} K_\psi T,$$

where K_ψ is universal (i.e., independent of microscopic details) within the scaling regime, and encodes the effect of the dissipative b -gauge fluctuations on heat transport.

For the spinon thermal conductivity, κ_f , in the presence of weak disorder (or any other mechanism that renders the dc response finite), the low-temperature spinon thermal conductivity takes the metallic form

$$\kappa_f = \gamma_f T,$$

a scaling that remains valid on both sides of the transition as long as the spinons retain a Fermi surface and transport is limited by elastic momentum relaxation. Approaching from the spinon-Fermi-liquid regime, the ratio κ_f/T is controlled by the Wiedemann–Franz relation for the spinon metal,

$$\frac{\kappa_f}{T} = L_0 \sigma_f, \quad L_0 = \frac{\pi^2}{3} \left(\frac{k_B}{e_*} \right)^2,$$

where σ_f is the residual *spinon* dc longitudinal conductivity, and e_* denotes the effective charge that couples the spinons to the probe driving the corresponding current.[43] At the critical point, additional inelastic scattering from the emergent b gauge fluctuations modifies the transport coefficients. In particular, the $T \rightarrow 0$ limit of κ_f/T acquires an extra universal contribution associated with the critical spinon–gauge-field sector, leading to a finite jump of the form

$$\frac{\kappa_f}{T} \Big|_{\text{QCP}} = \frac{\kappa_f}{T} \Big|_{\text{FL}} + \frac{k_B^2}{\hbar} K_f,$$

where K_f is a dimensionless constant determined by the interacting fixed point. Notably, in contrast to the corresponding charge transport, the spinon thermal conductivity remains finite on the spin-liquid side, and at low temperatures it is dominated by heat conduction in the coupled spinon– b -gauge-field sector.

Combining these two relations immediately implies a parametrically violated WF ratio (as emphasized in Refs. [26, 44]):

$$\frac{\kappa_{\text{tot}}}{T \sigma_{\text{tot}}} \simeq \frac{\kappa_\psi}{T \sigma_\psi} + \frac{\kappa_f}{T \sigma_\psi} = L_\psi + \frac{\gamma_f}{\sigma_\psi}.$$

Here $L_\psi \equiv \kappa_\psi/(T\sigma_\psi)$ is the effective Lorenz ratio of the charged Dirac sector alone (which need not equal the Fermi-liquid value L at criticality), and the second term is a strictly positive correction from the neutral spinons. Therefore, even if the charged sector by itself happened to exhibit an approximately constant Lorenz ratio, the presence of a sizable neutral heat channel generically enhances $\kappa/(T\sigma)$ and leads to a robust breakdown of the Wiedemann–Franz law in the total, physical response.

A quantitative calculation of κ_f can in principle be organized in a large- N expansion, or via an equivalent kinetic/memory-matrix formulation. While such approaches capture the expected scaling $\kappa_f \propto T$, obtaining the prefactor is technically nontrivial: gauge-mediated scattering is strongly forward-peaked, vertex corrections are essential, and a finite dc κ_f requires a consistent treatment of momentum relaxation (weak disorder/Umkapp) together with inelastic gauge fluctuations. A detailed microscopic computation of the prefactors is left for future work.

C. Experiment

Our results are directly applicable to TMD homobilayers and graphene moiré systems where the displacement field tunes the effective bandwidth [6, 7]. The predicted signature of the CFL-to-FL transition is a sharp enhancement in the longitudinal resistivity ρ_{xx} as the system passes through the critical point.

For the $\nu = -1/2$ transition, our calculation yields a critical contribution $\rho_\psi \approx 4.82 \hbar/e^2$. While the background resistivity ρ_f is metallic, the additive ρ_ψ creates a prominent peak at the critical tuning parameter. Furthermore, within the quantum critical fan, the scattering rate $\tau_{\text{tr}}^{-1} \sim T$ (Eq.34) governs the transport, leading to a universal DC resistivity, i.e., $\sigma_\psi \sim T \tau_{\text{tr}}$ is independent of T . However, we have to point out that, the “universality” only valid for low temperature where $T \ll \mu$ is held. Otherwise, the subleading term of T^2/μ order is not negligible and the conductivity will display a T^2 dependence. This is reflected on the QBE: our approximation for treating D_b is no longer acceptable and the Fermi surface terms may no longer be ignored. Hence the QBE needs to be carefully reformulated in this regime.

We also note that the critical point will be modified upon the inclusion of disorder and an intermediate CDW* phase will result, as discussed in Ref. [26]. Hence the calculation above applies to the clean limit.

VII. CONCLUSION

In this work we have presented a controlled analysis of universal electrical transport at continuous transitions between a composite Fermi liquid and a conventional metal (with a background integer quantum Hall state for $\nu = -3/4$) in moiré Chern bands, with explicit focus on fillings $\nu = -1/2$ and $\nu = -3/4$. Building on the parton-based critical theories proposed in Ref. [26], the low-energy description takes the form of a QED–Chern–Simons theory in which a critical charged sector—realizing a bosonic Laughlin–superfluid transition—is coupled, via emergent gauge fields and Chern–Simons mixing, to a neutral spinon Fermi surface.

A central technical result is the explicit derivation of an Ioffe–Larkin composition rule for the full electromagnetic

response. By integrating out matter fields to quadratic order and solving the resulting Gaussian gauge theory, we demonstrated that the physical resistivity tensor can be viewed as a series combination of the resistive channels associated with the critical charged sector and the neutral Fermi surface, while the Chern–Simons structure generates the Hall response. This formulation makes transparent how universal critical transport emerges, with coupling to a metallic spectator sector.

To access the d.c. conductivity in the quantum critical fan, where $\omega/T \rightarrow 0$, we developed a controlled large- N expansion in which both the number of fermion flavors and the Chern–Simons levels scale with N . Within this framework, the collisionless Drude singularity present at $N = \infty$ is removed at leading nontrivial order $O(1/N)$ by gauge-mediated inelastic scattering. Solving a quantum Boltzmann equation for the critical Dirac sector, we obtained a universal scaling function $\Sigma(\omega/T)$ and finite d.c. conductivities $\sigma(0) \approx 0.033(e^2/\hbar)$ for $\nu = -1/2$ and $\sigma(0) \approx 0.047(e^2/\hbar)$ for $\nu = -3/4$. These values represent universal numbers associated with the proposed CFL–metal critical points.

An important conceptual outcome of our analysis is the identification of a Chern–Simons “filtering” mechanism: although the neutral spinon Fermi surface strongly Landau-damps its associated gauge field, the Chern–Simons coupling suppresses the transmission of this damping to the critical gauge mode controlling charge transport. As a result, the spectrum of gauge boson b is not sharply peaked at $\omega = 0$, but rather broadened to a finite width, and the inelastic scattering process should be kept.

Our results provide concrete, experimentally accessible diagnostics for bandwidth-tuned transitions in moiré materials. In particular, the predicted universal resistivity platform in the quantum critical regime offer sharp signatures distinguishing the CFL–metal transition from adjacent Fermi-liquid phases. More broadly, the framework developed here parallels earlier universal-transport analyses of Mott criticality, while extending them to a setting enriched by topological response and emergent gauge structure. We expect that similar methods can be applied to other fractionalized quantum critical points in moiré systems and beyond. It would be interesting in the future to study the thermal conductivity in the proximity of the critical point, as similarly studied in a semiconductor metal-insulator transition[45].

ACKNOWLEDGMENT

The authors are particularly thankful to T Senthil and Haoyu Guo for suggesting this topic and helpful discussions. XYS is supported by the Croucher innovation awards and Area of Excellence scheme of RGC Hong Kong (AoE/P-604/25-R).

Appendix A: Analytical treatments of gauge polarization function

In this appendix, we will illustrate the analytical methods for solving equations of propagators, and express the gauge polarization function in terms of fermion bubble diagrams (Eq.12,13,14) for both case.

Due to current conservation, $P_\mu \Pi^{\mu\nu} = 0$, the polarization tensor admits the standard decomposition into transverse, longitudinal, and antisymmetric sectors,

$$\Pi^{\mu\nu}(P \equiv (\omega_n, \mathbf{p})) = \Pi_T P_T^{\mu\nu} + \Pi_L P_L^{\mu\nu} + \Pi_O P_O^{\mu\nu}, \quad (\text{A1})$$

where the projectors are defined by

$$P_T^{ij} = \delta^{ij} - \frac{p^i p^j}{P^2}, \quad P_T^{0\mu} = 0, \quad P_O^{\mu\nu} = \epsilon^{\mu\nu\lambda} \frac{P^\lambda}{P}, \quad (\text{A2})$$

$$P_L^{\mu\nu} = \delta^{\mu\nu} - E^{\mu\nu} - P_T^{\mu\nu}, \quad E^{\mu\nu} = \frac{P^\mu P^\nu}{P^2}. \quad (\text{A3})$$

Here P denotes the magnitude associated with the Euclidean three-momentum $P^\mu = (\omega_n, \mathbf{p})$, and the tensors $P_T^{\mu\nu}, P_L^{\mu\nu}$ project onto the spatially transverse and the remaining (gauge-invariant) longitudinal subspaces, while $P_O^{\mu\nu}$ captures the parity-odd (Hall/Chern-Simons) structure.

And we have $\mathbf{P} = \frac{P}{2\pi} P_O$, $\mathbf{P}' = \frac{P}{2\pi} P_O - \frac{1}{\epsilon} E$. We can extract these components via

$$\begin{aligned} \Pi_L &= \frac{P^2}{P^2} \Pi^{00}, & \Pi_T &= \Pi^{ii} - \frac{\omega_n^2}{P^2} \Pi^{00}, \\ \Pi_O &= \frac{P}{2\omega} (\Pi^{12} - \Pi^{21}). \end{aligned} \quad (\text{A4})$$

These relations follow by contracting $\Pi^{\mu\nu}$ with the corresponding projectors and using $P_\mu \Pi^{\mu\nu} = 0$ to eliminate redundant components. In practice, Eq. (A4) provides a convenient way to extract $\Pi_{T,L,O}$ directly from Π^{00} , Π^{ii} and the antisymmetric spatial part.

We can verify immediately that these tensors respect the following algebras:

$$P_T^2 = P_T, \quad P_L^2 = P_L, \quad E^2 = E, \quad P_O^2 = E - \delta, \quad (\text{A5})$$

$$P_O E = 0, \quad P_T P_L = 0, \quad P_T E = 0, \quad (\text{A6})$$

$$P_O P_T + P_T P_O = P_O, \quad P_O P_T P_O = -P_L. \quad (\text{A7})$$

These identities encode the mutual orthogonality of the transverse and longitudinal sectors, as well as the way the parity-odd structure mixes them. They are particularly useful for algebraic manipulations of quadratic actions and for inverting kernel operators written in the $(P_T, P_L, P_O, E, \delta)$ basis.

These algebras are derived following formula for the inverse of the general form of correlation functions:

$$\begin{aligned} (aP_T + bP_O + cE + d\delta)^{-1} &= \\ -\frac{1}{ad + b^2 + d^2} \left[aP_T + bP_O + \frac{cd + ca - b^2}{c + d} E - (a + d)\delta \right] \end{aligned} \quad (\text{A8})$$

which we repeatedly use to integrate out internal gauge fields and obtain the effective response kernel for the remaining mode.

1. $\nu = -1/2$ case

Inserting Eq.A8, Eq.(19) gives

$$\Pi_{b,T} = \frac{P^2 F_T - p^2 \Psi_T - 4\pi^2 f_l F_T \Psi_T}{P^2 + 4\pi^2 F_L F_T}, \quad (\text{A9})$$

$$\Pi_{b,L} = \frac{P^2 F_L - P^2 \Psi_L - 4\pi^2 F_L F_T \Psi_L}{P^2 + 4\pi^2 F_L F_T}, \quad (\text{A10})$$

$$\Pi_{b,O} = \frac{P^3}{2\pi P^2 + 8\pi^3 F_L F_T}. \quad (\text{A11})$$

where we denote $\Pi_{\psi/f}$ by Ψ/F respectively for compactness. Physically, Ψ encodes the critical Dirac sector response, while F captures the contribution from the Fermi-surface sector; together with the Chern-Simons structure they determine the full effective propagator for the emergent gauge mode b .

The three polarization components, $\Pi_{f,L}$ and $\Pi_{f,T}$, contributes by spinon Fermi surface are both proportional to chemical potential μ . Since $\omega, p, T \ll \mu$, we can insert the limit $\mu \rightarrow \infty$ in Eq.A9,A10,A11 and substitute them into Eq.22, obtaining

$$D_b = \text{Im}(1/\Psi_T) \quad (\text{A12})$$

This approximation corresponds to keeping only the dominant Fermi-surface contribution in the gauge dressing, which is justified for generic frequencies of order $\omega \sim p, T$ in the QC regime. In this regime, the dependence on microscopic Fermi-surface parameters enters only through the overall scale μ and drops out in the $\mu \rightarrow \infty$ limit, leaving a universal expression controlled by $\Pi_{\psi,T/L}$.

However, this one only hold for ω of normal scale, i.e., $\omega \sim p, T$. Note that for ω sufficiently small, specifically $\omega \sim T^2/\mu$, the dominance of μ terms is broken. More precisely, Eq.13 and Eq.14 at $T \ll \mu$ give the 2d Lindhard functions for $\omega < v_F p$:

$$\begin{cases} \Pi_{f,L}(\omega, p) = \frac{\mu}{\pi} \frac{\omega^2 - p^2}{v_F^2 p^2} \left(1 + i \frac{\omega}{\sqrt{v_F^2 p^2 - \omega^2}} \right) \\ \Pi_{f,T}(\omega, p) = \frac{\mu}{\pi} \left(\frac{\omega^2}{v_F^2 p^2} - i \frac{\omega}{\sqrt{v_F^2 p^2 - \omega^2}} \right) \end{cases}. \quad (\text{A13})$$

In particular, when $\omega \ll v_F p$, the imaginary parts encode Landau damping from the Fermi surface. From Eq.A13,

within the regime $\omega \ll p$, the imaginary part of propagator $D_b = 1/\Pi_{b,\text{eff}}$ might act as

$$\text{Im}D_b(\omega, p) \simeq \frac{\alpha\mu\omega + \beta\mu^3\omega^3}{X + Y\mu^2\omega^2 + Z\mu^4\omega^4}. \quad (\text{A14})$$

to the leading order of ω/μ (if the coupling is not exactly the Chern-Simons one), where α, β, X, Y, Z are some undetermined coefficients. Extracting a factor of ω , the remaining factor of the function displays a semi-singular peak at $\omega = 0$ with a height of order μ/p^2 and width of order p^2/μ , which will play the role of δ -function in the QBE. This function encodes the mode of Landau damping and is independent from the analytical part (Eq.A12) of D_b . We must handle its coefficients carefully. Fortunately, detailed calculations show that the imaginary contribution of the two terms from $\Pi_{b,\text{eff}} := \Pi_{b,T} + \Pi_{b,O}^2/\Pi_{b,L}$ canceled, implying the vanishing of Landau damping effect, which is nothing but a intrinsic manifestation of Chern-Simons coupling as we explained in Sec.IIB.

2. $\nu = -3/4$ case

For the case of $\nu = -3/4$, the propagator equation is much more involved. We read from the Feynman's rules that

$$\Delta_b^{-1} = -\mathbf{P}' - \Pi_\psi - \mathbf{P} \cdot \Delta_\alpha \cdot \mathbf{P}, \quad (\text{A15})$$

$$\Delta_a^{-1} = -\Pi_f - \mathbf{P} \cdot \Delta_\alpha \cdot \mathbf{P}, \quad (\text{A16})$$

$$\Delta_a^{-1} = -2\mathbf{P}' - \mathbf{P} \cdot \Delta_{b_1} \cdot \mathbf{P} - \mathbf{P} \cdot \Delta_{b_2} \cdot \mathbf{P} - \mathbf{P} \cdot \Delta_a \cdot \mathbf{P}, \quad (\text{A17})$$

$$\Delta_A^{-1} = -\mathbf{P} \cdot \Delta_\alpha \cdot \mathbf{P}, \quad (\text{A18})$$

which should be understood as *bookkeeping relations* indicating the possible dressing channels for each gauge field.

It should be noted that the above equations, when treated as a system, lacks physical meaning as it serves only as a hint for the types of dressing terms that can appear in each total propagator. This is because computing the total propagator for a field, say α , requires accounting for diagrams where α transforms into b and back into α , and where b may in turn transform back into α during the intermediate process, introducing an extra inner α line. Such diagrams violate one-particle irreducibility and must be excluded. In other words, when considering a b propagator within an α line, the Δ_α term in the equation for Δ_b^{-1} must be ignored. Equivalently, when constructing the effective quadratic kernel for a given field, only *one-particle-irreducible* (1PI) insertions with respect to that field should be retained; otherwise one double-counts self-energy insertions generated by repeated mixing through intermediate fields. Obeying these principles, we ultimately obtain Eq.(46). After repeated application of Eq.(A8) through lengthy calculations, we ultimately solve from Eq.(46) that

$$\Pi_{b,T}(P) = \frac{F_T (P^2 + 8\pi^2 F_L \Psi_T) (P^2 + 8\pi^2 \Psi_L \Psi_T) + P^2 \Psi_T (P^2 + 4\pi^2 (F_L + \Psi_L) \Psi_T)}{P^4 + 64\pi^4 F_L F_T \Psi_L \Psi_T + 4P^2 \pi^2 (F_L + \Psi_L) (F_T + \Psi_T)}, \quad (\text{A19})$$

$$\Pi_{b,L}(P) = \frac{F_L (P^2 + 8\pi^2 F_T \Psi_L) (P^2 + 8\pi^2 \Psi_L \Psi_T) + P^2 \Psi_L (P^2 + 4\pi^2 \Psi_L (F_T + \Psi_T))}{P^4 + 64\pi^4 F_L F_T \Psi_L \Psi_T + 4P^2 \pi^2 (F_L + \Psi_L) (F_T + \Psi_T)}, \quad (\text{A20})$$

$$\Pi_{b,O}(P) = \frac{P}{2\pi} - \frac{2\pi P F_L F_T (P^2 + 8\pi^2 \Psi_L \Psi_T)}{P^4 + 64\pi^4 F_L F_T \Psi_L \Psi_T + 4P^2 \pi^2 (F_L + \Psi_L) (F_T + \Psi_T)}. \quad (\text{A21})$$

Taking the limit $\mu \rightarrow \infty$ in Eq.[A19](#),[A20](#),[A21](#) and substitute them into Eq.[22](#), obtaining

$$D_b(\omega, p) = \text{Im} \left\{ \frac{(q^2 - \omega^2 + 8\pi^2 \Psi_T \Psi_L)}{\Psi_T [2(q^2 - \omega^2) + 8\pi^2 \Psi_T \Psi_L]} \right\} \quad (\text{A22})$$

Analogously, Landau damping does not apply on the low frequency region as in the $\nu = -1/2$ case, thus we do not need to concern about the semi-singularity near zero frequency.

Not surprisingly, all the Fermi surface information, such as v_F and k_F are blocked by this approach: in the regime of interest the dependence on the Fermi surface enters only through the large scale μ , and after taking the appropriate limits the resulting low-energy spectral weight relevant for our QBE analysis is controlled by universal combinations of $\Pi_{\psi,T}$ and $\Pi_{\psi,L}$.

Appendix B: Transport due to normal part of spectral function

In this Appendix, we present the details for linearizing the scattering terms associated with $\text{Im}D_b(\omega, p)$ of the gauge-boson spectral function. Our goal is to rewrite the collision integral in a form suitable for the linearized QBE, i.e. as a linear integral acting on the nonequilibrium distribution δf (or equivalently on the scalar function φ introduced in the main text).

We start from Eq.[30](#). Retaining the linear order of δf and integrating out frequency Ω , we obtain

$$I_b = -\frac{1}{N} \int \frac{d^2 q}{(2\pi)^2} \frac{(\mathbf{k} \times \hat{\mathbf{q}})^2}{2\epsilon_k \epsilon_{k'}} \times \left\{ D_b(|\epsilon_k - \epsilon_{k'}|, q) [\gamma(k, k') \delta f(k) - \gamma(k', k) \delta f(k')] + D_b(|\epsilon_k + \epsilon_{k'}|, q) [\Gamma(k, k') \delta f(k) - \Gamma(k', k) \delta f(k')] \right\}, \quad (\text{B1})$$

in which we denote $\mathbf{k}' = \mathbf{k} + \mathbf{q}$. Here the two terms in braces correspond to two distinct kinematic channels: the first involves energy transfer $|\epsilon_k - \epsilon_{k'}|$ (scattering with absorption/emission of a gauge boson), while the second involves $|\epsilon_k + \epsilon_{k'}|$ and describes processes that create or annihilate holon-doublon pairs. The prefactor $(\mathbf{k} \times \hat{\mathbf{q}})^2$ arises from the transverse gauge-vertex structure in Coulomb gauge and enforces that only momen-

tum components perpendicular to \mathbf{q} contribute to the integral.

The two gamma functions are defined by

$$\gamma(k, k') = \frac{[1 - n_F(k)] n_F(k')}{n_F(k') - n_F(k)}, \quad (\text{B2})$$

$$\Gamma(k, k') = \frac{[1 - n_F(k')] n_F(k')}{1 - n_F(k) - n_F(k')}, \quad (\text{B3})$$

which corresponding to the absorption and emission channel and the holon-doublon pairs channel respectively. These combinations are obtained after performing the frequency integral and collecting the remaining equilibrium distribution factors. In particular, γ is associated with the usual gain-loss structure for transitions between the single-particle states $k \rightarrow k'$, while Γ encodes the phase-space factor appropriate for the pair channel.

Inserting Eq.[32](#), Eq.[B1](#) can be further reorganized to a simpler form:

$$I_b = \frac{T}{N} \mathbf{E} \cdot \mathbf{k} \left[-F_b \left(\frac{k}{T} \right) \varphi(k) + \int \frac{dk'}{T} K_b(k', k) \varphi(k') \right]. \quad (\text{B4})$$

In this representation, the collision term is explicitly linear in the driving field \mathbf{E} and in the unknown function $\varphi(k)$, and it is separated into an “out-scattering” part proportional to $-F_b \varphi(k)$ and an “in-scattering” part represented by the integral kernel $K_b(k', k)$. The overall factor T/N reflects the large- N suppression of gauge scattering together with the thermal scaling inherited from the linearization around the Fermi distribution.

The function F_b and K_b can be written as follow:

$$F_b(k) = \int \frac{k' dk'}{2\pi} [f_1(k, k') |\gamma(k, k')| + f_2(k, k') \Gamma(k, k')], \quad (\text{B5})$$

$$K_b(k', k) = \frac{k'}{2\pi} [f_3(k', k) |\gamma(k', k)| - f_4(k', k) \Gamma(k, k')], \quad (\text{B6})$$

where the angular dependence of the scattering has been integrated out and absorbed into the functions $f_{1,2,3,4}$. Concretely, F_b collects all contributions in which the distribution distortion is evaluated at the same momentum k , whereas K_b multiplies $\varphi(k')$ and describes scattering into the state k from all other k' .

The four f s are angular avaraged functions defined as

$$f_1(k, k') = - \int_0^{2\pi} \frac{d\theta}{2\pi} D_b(|k - k'|, |\mathbf{k} + \mathbf{k}'|) \frac{kk' \sin^2 \theta}{2(\mathbf{k} + \mathbf{k}')^2}, \quad (B7)$$

$$f_2(k, k') = - \int_0^{2\pi} \frac{d\theta}{2\pi} D_b(k + k', |\mathbf{k} + \mathbf{k}'|) \frac{kk' \sin^2 \theta}{2(\mathbf{k} + \mathbf{k}')^2}, \quad (B8)$$

$$f_3(k, k') = - \int_0^{2\pi} \frac{d\theta}{2\pi} D_b(|k - k'|, |\mathbf{k} + \mathbf{k}'|) \frac{kk' \cos \theta \sin^2 \theta}{2(\mathbf{k} + \mathbf{k}')^2}, \quad (B9)$$

$$f_4(k, k') = - \int_0^{2\pi} \frac{d\theta}{2\pi} D_b(k + k', |\mathbf{k} + \mathbf{k}'|) \frac{kk' \cos \theta \sin^2 \theta}{2(\mathbf{k} + \mathbf{k}')^2}. \quad (B10)$$

where θ is the angle between \mathbf{k} and \mathbf{k}' . The factors of $\sin^2 \theta$ (and $\cos \theta \sin^2 \theta$ in $f_{3,4}$) originate from the transverse gauge vertex and from projecting the vector structure of the collision integral onto the $\mathbf{E} \cdot \mathbf{k}$ driving term, ensuring that the resulting kernel respects rotational invariance.

Appendix C: Current polarization function of Dirac fermion

In this appendix, we will give a single-variable integral form of the current polarization functions, which are more convenient for numerical processing. The gauge polarization functions of the Dirac fermion ψ can be expressed in terms of the diagonal components:

$$\Psi_{ii}(\nu_l, p) = \int_{\mathbf{k}, \omega_n} \frac{4\omega_n(\omega_n + \nu_l)}{(\mathbf{k}^2 + \omega_n^2)[(\mathbf{k} + \mathbf{p})^2 + (\omega_n + \nu_l)^2]}, \quad (C1)$$

$$\Psi_{00}(\nu_l, p) = \int_{\mathbf{k}, \omega_n} \frac{2[\mathbf{k} \cdot (\mathbf{k} + \mathbf{p}) - \omega_n(\omega_n + \nu_l)]}{(\mathbf{k}^2 + \omega_n^2)[(\mathbf{k} + \mathbf{p})^2 + (\omega_n + \nu_l)^2]}, \quad (C2)$$

where $\int_{\mathbf{k}, \omega_n} := T \sum_{\omega_n} \int \frac{d^2 \mathbf{k}}{(2\pi)^2}$. These expressions follow from Eq.12 together with Eq.A8, after projecting the tensor structure onto the corresponding components.

Carrying out the Matsubara-frequency summation, we obtain the thermal part which is proportional to $n_F(\beta k)$ and the vacuum part which is thermal-independent of polarization function. The vacuum part has been well-studied (see, e.g.,[33]) and can be regulated to $\Psi_T^{\text{vac}} = \Psi_L^{\text{vac}} = \sqrt{q^2 - \omega^2}/16$, while the thermal parts are evaluated to be

$$\Psi_{ii}(\omega, p) = \int \frac{d^2 \mathbf{k}}{(2\pi)^2} \left\{ \frac{4(k - \omega)n_F(\beta k)}{p^2 + (2k - \omega)\omega + 2kp \cos \theta} + \frac{4(k + \omega)n_F(\beta k)}{-p^2 + \omega(2k + \omega) + 2kp \cos \theta} \right\}, \quad (C3)$$

$$\Psi_{00}(\omega, p) = \int \frac{d^2 \mathbf{k}}{(2\pi)^2} \left\{ \frac{2(2k + \omega + p \cos \theta)n_F(\beta k)}{-p^2 + \omega(2k + \omega) + 2kp \cos \theta} - \frac{2(2k - \omega + p \cos \theta)n_F(\beta k)}{p^2 + (2k - \omega)\omega + 2kp \cos \theta} \right\}. \quad (C4)$$

In the above, ω has already been analytically continued from the Matsubara frequency ν_l to the real axis, with the standard retarded prescription $\omega \rightarrow \omega + i0^+$. This continuation fixes the branch of the square roots below and determines the real/imaginary parts.

Note that the expression for Ψ_{00} contains an UV divergent contribution proportional to $1/k$. This term is removed after regularization.

After performing the angular integral over θ , one arrives at one-dimensional radial integrals:

$$\begin{aligned} \Psi_{ii}(\omega, p) = & \int \frac{k dk}{2\pi} \left\{ \frac{\text{sign}(s)2(k - \omega)}{\sqrt{[p^2 - (2k - \omega)^2](p^2 - \omega^2)}} \right. \\ & \left. + \frac{\text{sign}(t)2(k + \omega)}{\sqrt{[p^2 - (2k + \omega)^2](p^2 - \omega^2)}} \right\} 2n_F(\beta k), \end{aligned} \quad (C5)$$

$$\begin{aligned} \Psi_{00}(\omega, p) = & - \int \frac{k dk}{2\pi} \left\{ \frac{\text{sign}(s) \left[2(k - \omega) + \frac{\omega^2 - p^2}{2k} \right]}{\sqrt{[p^2 - (2k - \omega)^2](p^2 - \omega^2)}} \right. \\ & \left. + \frac{\text{sign}(t) \left[2(k + \omega) + \frac{\omega^2 - p^2}{2k} \right]}{\sqrt{[p^2 - (2k + \omega)^2](p^2 - \omega^2)}} \right\} 2n_F(\beta k), \end{aligned} \quad (C6)$$

where $s = p^2 + (2k - \omega)\omega$, $t = p^2 - \omega(2k + \omega)$.

For numerical evaluation it is convenient to explicitly separate the real and imaginary parts. Using the retarded prescription to resolve the branch cuts, we decompose

$$\begin{aligned} \text{Re}\Psi_{ii}(\omega, p) = & \int \frac{k dk}{2\pi} \left[2(k - \omega)\text{sign}(s) \right. \\ & \times \frac{\Theta(p - \omega)\Theta(p - |x|) + \Theta(\omega - p)\Theta(|x| - p)\text{sign}(x)}{\sqrt{|p^2 - \omega^2||x^2 - p^2|}} \\ & \left. + 2(k + \omega)\text{sign}(t) \right. \\ & \times \frac{\Theta(p - \omega)\Theta(p - y) - \Theta(\omega - p)\Theta(y - p)}{\sqrt{|p^2 - \omega^2||y^2 - p^2|}} \left. \right] 2n_F(\beta k), \end{aligned} \quad (C7)$$

$$\begin{aligned}
\text{Im}\Psi_{ii}(\omega, p) = & \int \frac{k dk}{2\pi} \left[2(k - \omega) \text{sign}(s) \right. \\
& \times \frac{\Theta(\omega - p)\Theta(p - |x|) - \Theta(p - \omega)\Theta(|x| - p)\text{sign}(x)}{\sqrt{|p^2 - \omega^2||x^2 - p^2|}} \\
& + 2(k + \omega)\text{sign}(t) \\
& \times \left. \frac{\Theta(\omega - p)\Theta(p - y) + \Theta(p - \omega)\Theta(y - p)}{\sqrt{|p^2 - \omega^2||y^2 - p^2|}} \right] 2n_F(\beta k),
\end{aligned} \tag{C8}$$

and similarly

$$\begin{aligned}
\text{Re}\Psi_{00}(\omega, p) = & - \int \frac{k dk}{2\pi} \left[\left(2k - 2\omega + \frac{\omega^2 - p^2}{2k} \right) \text{sign}(s) \right. \\
& \times \frac{\Theta(p - \omega)\Theta(p - |x|) + \Theta(\omega - p)\Theta(|x| - p)\text{sign}(x)}{\sqrt{|p^2 - \omega^2||x^2 - p^2|}} \\
& + \left. \left(2k + 2\omega + \frac{\omega^2 - p^2}{2k} \right) \text{sign}(t) \right. \\
& \times \left. \left. \frac{\Theta(p - \omega)\Theta(p - y) - \Theta(\omega - p)\Theta(y - p)}{\sqrt{|p^2 - \omega^2||y^2 - p^2|}} \right] 2n_F(\beta k),
\end{aligned} \tag{C9}$$

$$\begin{aligned}
\text{Im}\Psi_{00}(\omega, p) = & - \int \frac{k dk}{2\pi} \left[\left(2k - 2\omega + \frac{\omega^2 - p^2}{2k} \right) \text{sign}(s) \right. \\
& \times \frac{\Theta(\omega - p)\Theta(p - |x|) - \Theta(p - \omega)\Theta(|x| - p)\text{sign}(x)}{\sqrt{|p^2 - \omega^2||x^2 - p^2|}} \\
& + \left. \left(2k + 2\omega + \frac{\omega^2 - p^2}{2k} \right) \text{sign}(t) \right. \\
& \times \left. \left. \frac{\Theta(\omega - p)\Theta(p - y) + \Theta(p - \omega)\Theta(y - p)}{\sqrt{|p^2 - \omega^2||y^2 - p^2|}} \right] 2n_F(\beta k).
\end{aligned} \tag{C10}$$

where $x = 2k - \omega$, $y = 2k + \omega$ and Θ is the step function. With these explicit forms, the remaining k integrals are well-suited for direct numerical evaluation. Here we show the density plot of $-\text{Im}(1/\Psi_T)$ (Fig. 5).

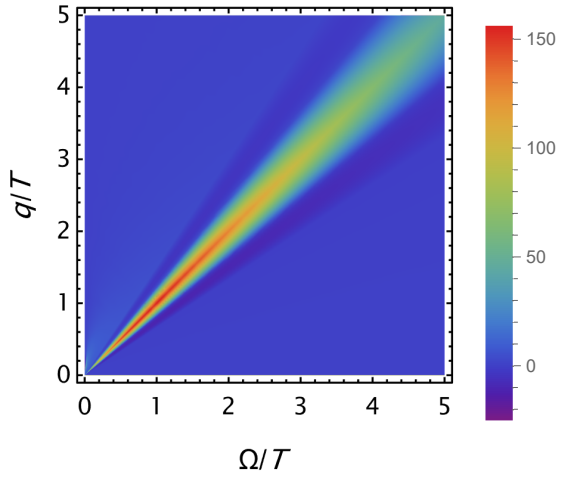


FIG. 5: Density plot of $-\text{Im}[1/\Psi_T(\Omega, q)]$.

[1] T. Li, S. Jiang, B. Shen, Y. Zhang, L. Li, Z. Tao, T. Devakul, K. Watanabe, T. Taniguchi, L. Fu, J. Shan, and K. F. Mak, Quantum anomalous Hall effect from intertwined moiré bands, *Nature* **600**, 641 (2021).

[2] B. A. Foutty, C. R. Kometter, T. Devakul, A. P. Reddy, K. Watanabe, T. Taniguchi, L. Fu, and B. E. Feldman, Mapping twist-tuned multiband topology in bilayer wse 2, *Science* **384**, 343–347 (2024).

[3] K. P. Nuckolls, M. Oh, D. Wong, B. Lian, K. Watanabe, T. Taniguchi, B. A. Bernevig, and A. Yazdani, Strongly correlated chern insulators in magic-angle twisted bilayer graphene, *Nature* **588**, 610 (2020).

[4] J. Cai, E. Anderson, C. Wang, X. Zhang, X. Liu, W. Holtzmann, Y. Zhang, F. Fan, T. Taniguchi, K. Watanabe, Y. Ran, T. Cao, L. Fu, D. Xiao, W. Yao, and X. Xu, Signatures of fractional quantum anomalous Hall states in twisted MoTe2, *Nature* **622**, 63 (2023).

[5] Y. Zeng, Z. Xia, K. Kang, J. Zhu, P. Knüppel, C. Vaswani, K. Watanabe, T. Taniguchi, K. F. Mak, and J. Shan, Thermodynamic evidence of fractional Chern insulator in moiré MoTe2, *Nature* **622**, 69 (2023).

[6] H. Park, J. Cai, E. Anderson, Y. Zhang, J. Zhu, X. Liu, C. Wang, W. Holtzmann, C. Hu, Z. Liu, T. Taniguchi, K. Watanabe, J.-H. Chu, T. Cao, L. Fu, W. Yao, C.-Z. Chang, D. Cobden, D. Xiao, and X. Xu, Observation of fractionally quantized anomalous hall effect, *Nature* **622**, 74 (2023).

[7] Z. Lu, T. Han, Y. Yao, A. P. Reddy, J. Yang, J. Seo, K. Watanabe, T. Taniguchi, L. Fu, and L. Ju, Fractional quantum anomalous hall effect in multilayer graphene, *Nature* **626**, 759 (2024).

[8] Y.-H. Zhang, D. Mao, Y. Cao, P. Jarillo-Herrero, and

T. Senthil, Nearly flat chern bands in moiré superlattices, *Physical Review B* **99**, 075127 (2019).

[9] P. J. Ledwith, G. Tarnopolsky, E. Khalaf, and A. Vishwanath, Fractional chern insulator states in twisted bilayer graphene: An analytical approach, *Phys. Rev. Res.* **2**, 023237 (2020).

[10] C. Repellin and T. Senthil, Chern bands of twisted bilayer graphene: Fractional chern insulators and spin phase transition, *Physical Review Research* **2**, 023238 (2020).

[11] A. Abouelkomsan, Z. Liu, and E. J. Bergholtz, Particle-hole duality, emergent fermi liquids, and fractional chern insulators in moiré flatbands, *Physical review letters* **124**, 106803 (2020).

[12] P. Wilhelm, T. C. Lang, and A. M. Läuchli, Interplay of fractional chern insulator and charge density wave phases in twisted bilayer graphene, *Physical Review B* **103**, 125406 (2021).

[13] F. Wu, T. Lovorn, E. Tutuc, I. Martin, and A. MacDonald, Topological insulators in twisted transition metal dichalcogenide homobilayers, *Physical review letters* **122**, 086402 (2019).

[14] H. Yu, M. Chen, and W. Yao, Giant magnetic field from moiré induced berry phase in homobilayer semiconductors, *National Science Review* **7**, 12 (2020).

[15] T. Devakul, V. Crépel, Y. Zhang, and L. Fu, Magic in twisted transition metal dichalcogenide bilayers, *Nature communications* **12**, 6730 (2021).

[16] H. Li, U. Kumar, K. Sun, and S.-Z. Lin, Spontaneous fractional chern insulators in transition metal dichalcogenide moiré superlattices, *Physical Review Research* **3**, L032070 (2021).

[17] V. Crépel and L. Fu, Anomalous hall metal and fractional chern insulator in twisted transition metal dichalcogenides, *Phys. Rev. B* **107**, L201109 (2023).

[18] X.-Y. Song, C.-M. Jian, L. Fu, and C. Xu, Intertwined fractional quantum anomalous hall states and charge density waves, *Phys. Rev. B* **109**, 115116 (2024).

[19] L. Zhang and X.-Y. Song, Moore-read state in half-filled moiré chern band from three-body pseudopotential, *Phys. Rev. B* **109**, 245128 (2024).

[20] X.-Y. Song and T. Senthil, Density wave halo around anyons in fractional quantum anomalous hall states, *Phys. Rev. B* **110**, 085120 (2024).

[21] Z. D. Shi and T. Senthil, Doping a fractional quantum anomalous hall insulator, *Phys. Rev. X* **15**, 031069 (2025).

[22] M. Kim, A. Timmel, L. Ju, and X.-G. Wen, Topological chiral superconductivity beyond pairing in a fermi liquid, *Phys. Rev. B* **111**, 014508 (2025).

[23] J. Dong, J. Wang, P. J. Ledwith, A. Vishwanath, and D. E. Parker, Composite fermi liquid at zero magnetic field in twisted mote _2, arXiv preprint arXiv:2306.01719 (2023).

[24] H. Goldman, A. P. Reddy, N. Paul, and L. Fu, Zero-field composite fermi liquid in twisted semiconductor bilayers, arXiv preprint arXiv:2306.02513 (2023).

[25] H. Park, J. Cai, E. Anderson, Y. Zhang, J. Zhu, X. Liu, C. Wang, W. Holtzmann, C. Hu, Z. Liu, T. Taniguchi, K. Watanabe, J.-H. Chu, T. Cao, L. Fu, W. Yao, C.-Z. Chang, D. Cobden, D. Xiao, and X. Xu, Observation of fractionally quantized anomalous Hall effect, *Nature* **622**, 74 (2023).

[26] X.-Y. Song, Y.-H. Zhang, and T. Senthil, Phase transitions out of quantum Hall states in moiré materials, *Physical Review B* **109**, 085143 (2024).

[27] T. Senthil, M. Vojta, and S. Sachdev, Weak magnetism and non-Fermi liquids near heavy-fermion critical points, *Physical Review B* **69**, 035111 (2004).

[28] T. Senthil, Theory of a continuous Mott transition in two dimensions, *Physical Review B* **78**, 045109 (2008).

[29] B. I. Halperin, P. A. Lee, and N. Read, Theory of the half-filled Landau level, *Physical Review B* **47**, 7312 (1993).

[30] M. Barkeshli and J. McGreevy, Continuous transitions between composite Fermi liquid and Landau Fermi liquid: A route to fractionalized Mott insulators, *Physical Review B* **86**, 075136 (2012).

[31] W. Chen, M. P. A. Fisher, and Y.-S. Wu, Mott transition in an anyon gas, *Physical Review B* **48**, 13749 (1993).

[32] X.-G. Wen and Y.-S. Wu, Transitions between the quantum Hall states and insulators induced by periodic potentials, *Physical Review Letters* **70**, 1501 (1993).

[33] S. Rao and R. Yahalom, Parity anomalies in gauge theories in 2 + 1 dimensions, *Physics Letters B* **172**, 227 (1986).

[34] T. Senthil, A. Vishwanath, L. Balents, S. Sachdev, and M. P. A. Fisher, Deconfined Quantum Critical Points, *Science* **303**, 1490 (2004).

[35] T. Senthil, Deconfined quantum critical points: a review (2023), arXiv:2306.12638 version: 2.

[36] T. Senthil, D. T. Son, C. Wang, and C. Xu, Duality between (2+1) d quantum critical points, *Physics Reports* **827**, 1 (2019).

[37] K. Damle and S. Sachdev, Nonzero-temperature transport near quantum critical points, *Physical Review B* **56**, 8714 (1997).

[38] S. Sachdev, Nonzero-temperature transport near fractional quantum Hall critical points, *Physical Review B* **57**, 7157 (1998).

[39] L. Fritz, J. Schmalian, M. Müller, and S. Sachdev, Quantum critical transport in clean graphene, *Physical Review B* **78**, 085416 (2008).

[40] W. Witczak-Krempa, P. Ghaemi, T. Senthil, and Y. B. Kim, Universal transport near a quantum critical Mott transition in two dimensions, *Physical Review B* **86**, 245102 (2012).

[41] L. B. Ioffe and A. I. Larkin, Gapless fermions and gauge fields in dielectrics, *Physical Review B* **39**, 8988 (1989).

[42] R. K. Kaul and S. Sachdev, Quantum criticality of U(1) gauge theories with fermionic and bosonic matter in two spatial dimensions, *Physical Review B* **77**, 155105 (2008).

[43] For electrically neutral spinons, σ_f here should be understood as the conductivity for the conserved spinon current (or, equivalently, the diffusion constant via the Einstein relation), rather than the physical electrical conductivity.

[44] C. Wang and T. Senthil, Half-filled landau level, topological insulator surfaces, and three-dimensional quantum spin liquids, *Physical Review B* **93**, 085110 (2016).

[45] A. C. Potter, M. Barkeshli, J. McGreevy, and T. Senthil, Quantum spin liquids and the metal-insulator transition in doped semiconductors, *Phys. Rev. Lett.* **109**, 077205 (2012).